Photo-excitation band-structure engineering of *2H*-$NbSe_2$ probed by time- and angle-resolved photoemission spectroscopy

Mari Watanabe
Tokyo University of Science
Takeshi Suzuki (takeshi.suzuki@issp.u-tokyo.ac.jp)
The University of Tokyo
Takashi Someya
The University of Tokyo
Yu Ogawa
The University of Tokyo
Shoya Michimae
The University of Tokyo
Masami Fujisawa
The University of Tokyo
Teruto Kanai
The University of Tokyo
Jiro Itatani
The University of Tokyo
Tomohiko Saitoh
Tokyo University of Science
Shik Shin
The University of Tokyo
Kozo Okazaki
The University of Tokyo

Research Article

Keywords: 2H-NbSe2, photoemission spectroscopy, electronic state

Posted Date: April 21st, 2021

DOI: https://doi.org/10.21203/rs.3.rs-428191/v1

Abstract

We investigated the nonequilibrium electronic structure of 2*H*-$NbSe_2$ by time- and angle-resolved photoemission spectroscopy. We find that the band structure is distinctively modulated by strong photo-excitation, as indicated by the unusual increase in the photoelectron intensities around E_F. In order to gain insight into the observed photo-induced electronic state, we performed DFT calculations with modulated lattice structures, and found that the variation of the Se height from the Nb layer results in a significant change in the effective mass and band gap energy. We further study the momentum-dependent carrier dynamics. The results suggest that the relaxation is faster at the K-centered Fermi surface than at the G-centered Fermi surface, which can be attributed to the stronger electron-lattice coupling at the K-centered Fermi surface. Our demonstration of band structure engineering suggests a new role for light as a tool for controlling the functionalities of solid-state materials.

Main Text

Engineering the band structure is a key method for changing the physical properties of solid-state materials. For example, increasing the effective mass significantly increases the electronic heat capacity and magnetic susceptibility [1] [2], while controlling the size of the band gap can tune the absorption and emission spectra [3]. These modifications have conventionally been performed by elemental substitution or applying physical pressure. Photo-excitation has substantial advantages over these methods because the physical properties of materials can be changed without any physical contact or further fabrication [4] [5] [6]. Furthermore, by using ultrashort pulses, material functionalities can be immediately activated. Therefore, photo-excitation has substantial potential for future applications in ultrafast electrical switching [7] [8] [9] [10].

The family of transition metal dichalcogenides (TMDCs) provides rich physics as materials for investigation due to the subtle balance between multiple competing orders such as the Mott insulator, charge density wave (CDW), and superconducting states [11]. This balance can be fairly easily broken by physical pressure [12] [13] or processing into few-layer structures [14] [15]. Photo-excitation has also been frequently employed to reveal hidden properties which do not appear under equilibrium conditions [16].

Among the TMDC materials, 2*H*-$NbSe_2$ has attracted significant interest because it possesses a unique profile in which the CDW and superconducting orders coexist. Figure 1(a) shows the crystal structure of 2*H*-$NbSe_2$. At room temperature, 2*H*-$NbSe_2$ is metallic owing to its half-filled dz^2 band. With decreasing temperature, it undergoes a CDW transition at 33 K [17] with the CDW vector, $\boldsymbol{q}$, of 2/3ΓM [18], and a superconducting transition at 7 K [19]. With regard to the CDW phase, two previous static angle-resolved photoemission spectroscopy (ARPSE) studies have reported different momentum dependences of the CDW gap size. One study showed that the CDW gap size is the largest along the MK direction and the smallest along ΓK [20]. This observation is not consistent with the nesting of the Fermi surface (FS), and suggests the possibility of another origin for the CDW gap anisotropy in 2*H*-$NbSe_2$. In contrast, another

study reported that the CDW gap opens along ΓK [21]. Thus, the origin of the CDW in 2*H*-$NbSe_2$ remains unclear. These contradicting reports indicate that another approach beyond static ARPES is required.

A non-equilibrium profile obtained using pump-probe type measurements can offer richer information not accessible by static measurements [22] [23]. Time- and angle-resolved photoemission spectroscopy (TARPES) is a very powerful technique for investigating momentum-dependent non-equilibrium behavior which can temporally track the photo-excited electronic band structure [24] [25] [10]. This technique has been successfully applied to other TMDC systems in which the time-domain observations revealed the excitonic nature of 1*T*-$TiSe_2$ [26] and the insulating nature of 1*T*-TaS_2 [27].

In this work, we use TARPES to study the nonequilibrium electronic states in 2*H*-$NbSe_2$ driven by photo-excitations. We find that photo-excitation induces a significant change in the effective mass and band gap energy. To confirm that the observed change in the electronic band structure is caused by the displacive excitation of coherent phonon (DECP) mechanism [28], we perform DFT calculations with modulated lattice structures. Furthermore, we study the electron-lattice couplings by measuring the momentum dependence of the electronic dynamical properties. The results suggest stronger electron-lattice couplings on the K-centered FS.

We first performed static ARPES measurements on 2*H*-$NbSe_2$ to confirm the orientation of the cleaved surface. Figure 1(b) shows the results of the FS mapping. The integrated energy window is ±10 meV from the Fermi level (E_F). The clear six-fold symmetry of the FS allows us to discern the specific symmetry points in momentum space shown in Fig. 1(b).

After confirming the sample orientation by static ARPES, we investigated the relaxation dynamics of the photo-excited electrons at the G-centered FS. Figure 1(c) shows the temporal evolution of the momentum-integrated energy distribution curves (EDCs) integrated along the ΓK direction indicated by the red line in Fig. 1(b). After the arrival of the pump pulses, electrons are immediately excited above E_F and relax to their original state. To provide more clarity, Fig. 1(d) shows the difference spectrum obtained by subtracting the average spectrum before the arrival of pump pulses from the EDCs. The red and blue colors correspond to increases and decreases in the intensities of the photoelectrons, respectively. It should be noted that in addition to the rapid rise and relaxation dynamics far above E_F, the intensity around E_F also increases after photo-excitation. Furthermore, the intensity at 0.5 eV *below* E_F also increases. This is quite striking because the electrons are transferred from the occupied to unoccupied states by photo-excitation, and thus the intensity of photoelectrons below E_F should generally decrease after the photo-excitation. This strange behavior indicates a change in the density of states (DOS) as a result of the change in the band structures. Additionally, this change persists for longer than 1 ps. Considering previous reports on the fairly short lifetime of approximately 1 ps of the photo-excited state in a metallic system [30], the observed slow relaxation dynamics show that the photo-induced state in 2*H*-$NbSe_2$ is unusually stable (meta-stable).

To investigate the origin of the unique observed change in the DOS and the long lifetime of the photo-induced state, we measured the momentum-resolved time-dependent band structure along the same cut in energy and momentum space. Figures 2(a)–2(e) show temporal snapshots of the *E-k* map at the indicated delay times (Δt). The difference spectra are also shown in Figs. 2(f)–2(j), where red and blue correspond to increases and decreases in the photoelectron intensities, respectively. Just after the pump at Δt = 13.3 and 40 fs, the unoccupied electron bands at around E - E_F = 1.3 eV become populated, as indicated by the white dashed circle in Fig. 2(b). This population is transiently observed and disappears at 93 fs. Focusing on the occupied bands, the original hole-like band corresponding to the blue regions in Figs. 2(g)-2(j) is split, as indicated by the two red regions in Figs. 2(g)–2(j). This striking change is most evident at Δt = 93 fs and is indicated by the two black dashed circles in Fig. 2(i).

We now discuss the observed changes in the band structure. Figures 3(a) and 3(b) show the *E-k* maps before and after photo-excitation as the difference spectra, respectively. It can be clearly seen that the hole band separates after photo-excitation and appears as a double-sided red region. This observation is most often explained as a consequence of the thermal effects due to the excitation pump. If the electronic temperature in 2*H*-$NbSe_2$ increases above the CDW transition temperature of 33 K, the material would show a phase transition from the CDW phase to the normal metallic phase. In this case, the band structure should show a change similar to that of the phase transition. However, according to previous studies [20] [21], the observed photo-induced state is completely different from the high-temperature band structure, which does not accompany the observed photo-induced change. We further performed TARPES measurements at a higher temperature of 40 K (>T_{CDW}), as shown in Fig. S1 [31]. Surprisingly, we observed qualitatively similar behavior to that at 15 K, which suggests that the temperature and CDW phase are largely irrelevant to the observed band changes. Thus, the thermal effect is not a plausible explanation for the observed state.

We suggest an alternative explanation whereby the rearrangement of the electron and lattice structure, as described by the DECP mechanism, is the driving force for the observed photo-induced state. In this rearrangement, near-infrared pulses first transfer the electronic population from the occupied to unoccupied states, and then cause lattice modulation. The electronic band structures are in turn modified and become coordinated with the modulated lattice structure. The absence of coherent phonons in our measurement is explained by the insufficient time resolution of our setup, which is approximately 80 fs. The frequency of coherent phonons corresponding to the stretching mode of Se atoms is 7 THz [32] [33], and thus the time resolution should be better than 35 fs, corresponding to a quarter of the oscillation period. Another reason for the absence of coherent phonons is their strong damping, which prevents their observation over multiple cycles.

To investigate the photo-induced electronic band structure caused by the lattice modulation corresponding to the A_{1g} phonon, we performed DFT calculations within the generalized gradient approximation. Figure 3(c) shows the calculated band structure of 2*H*-$NbSe_2$ with the structure at equilibrium. The Nb 4*d* and Se 4*p* bands lie close to each other along the ΓK direction. To see how this

electronic band structure is affected by lattice modulation, we performed DFT calculations on structures with various heights of the Se away from the nearest Nb layer. Figure 3(d) shows the calculation results for the modulated structures schematically shown in Fig. 3(e). Figure 3(f) shows the magnified band structure corresponding to the area indicated by the gray hatch in Fig. 3(d). It should be noted that the effective mass of the Se 4*p* valence bands changes significantly with increasing Se height. The mechanism behind the observed photo-induced evolution of the TARPES spectra can be understood based on these calculation results. Photo-excitation can change the height of Se in line with the DECP mechanism. This lattice change leads to an increase in the effective mass of the Se 4*p* band, which results in the separation of the Se 4*p* band from the Nb 4*d* band, as shown in Figs. 2(i) and 3(b), and an increase in the DOS around E_F, as shown in Fig. 1(d). It is also noted that the unoccupied bands shift toward lower energies at the larger lattice modulations shown as circles in Fig. 3(d). This change suggests that the transient population in the unoccupied band shown as the dashed circle in Fig. 2(b) can be considered to be a result of the decrease in the band gap caused by the photo-induced change of the lattice structure.

Finally, we discuss the momentum-dependent dynamical behavior and infer its relationship to the CDW gap anisotropy. To investigate the momentum-dependent non-equilibrium properties, we measured the time-dependent photoemission intensities of the FSs around the Γ and K points, and compared the results. Figure 4(a) shows the time-dependent momentum-integrated photoemission intensities of the FSs around the Γ and K points as the red and green markers, respectively. The momentum cuts for the FSs around the Γ and K points are shown as red and green solid lines in Fig. 4(b). To gain a quantitative insight, we fit the experimental data by a single exponential decay function convoluted with a Gaussian function. The fits are shown as red and green solid lines for the FSs around the Γ and K points, respectively. The decay constants of the FSs at the Γ and K points are 78 and 46 fs, respectively while the Gaussian wiΔths are 39 and 48 fs for around the Γ and K points, respectively. According to the two-temperature model, the pump pulse injects excess energy into the electron system. The energy is then transferred to the lattice system via electron-lattice coupling. The speed of the energy transfer is determined by the electron-lattice coupling constant. The larger the electron-lattice coupling constant, the faster the excess energy is transferred to the lattice system. Our finding of the faster decay of the photoemission intensities of the FS at the K point, which reflects the faster hot carrier dynamics, indicates a stronger electron-lattice coupling.

With regard to the CDW gap anisotropy, the stronger electron-lattice coupling around the K point favors the result of Ref. [21]. However, the carrier dynamics are affected by many factors other than the amplitude of the gap, such as the size of the FS and the populations of the involved phonons. Further studies following the present work will be required.

We studied the photo-induced electronic states in 2*H*-$NbSe_2$ by TARPES. We found distinctive changes in the electronic profile manifested as the persistent increase of photoelectrons around E_F and the separation of the Se *4p* band from the Nb *4d* band as a result of an increase in the effective mass of the Se *4p* band. This unusual state is induced by the lattice modulation in line with the DECP mechanism,

and confirmed by DFT calculations. We further investigated the momentum-dependent dynamics. The dynamics indicate a larger electron-lattice coupling at the K point.

Methods

Static angle-resolved photoemission spectroscopy

For the static ARPES, we used a photon energy of 21.2 eV obtained from a He-I lamp (Scienta Omicron VUV 5050), and detected the photoelectrons using a Scienta R4000 analyzer.

Time- and angle-resolved photoemission spectroscopy

In the TARPES setup, we used a Ti:sapphire laser system (Coherent Astrella) with a pulse width of 35 fs, center wavelength of 800 nm (1.55 eV), and repetition rate of 1 kHz. The laser pulses were split into pump and probe pulses. For the pump pulses, we used the fundamental wavelength and set the fluence to 2 mJ/cm^2. For the probe pulses, we first doubled the photon energy to 3.10 eV using a β-BaB_2O_4 crystal, and then focused the pulses on the Ar gas filled in the gas cell to achieve high-harmonic generation. We selected the 9th harmonic corresponding to 27.9 eV using a pair of SiC/Mg multilayer mirrors. By using such a high photon energy for the probe pulses, the entire Brillouin zone of 2*H*-$NbSe_2$ can be captured. We estimated the temporal resolution to be less than 80 fs by measuring the response time of highly-oriented pyrolytic graphite and an energy resolution of 250 meV by measuring the energy distribution curves (EDCs) for bulk gold. All the measurements in this study were carried out at the temperature of 15 K unless otherwise stated.

Sample

High-quality single crystals of 2*H*-$NbSe_2$ were provided by HG Graphene. Clean surfaces were obtained by cleaving *in situ*.

Band structure calculations

Band structure calculations based on density functional theory (DFT) were performed using the WIEN2k package [29]. a = 3.45 Å and c = 12.54 Å were used for the lattice parameters in the equilibrium state [11].

Declarations

Acknowledgements

We would like to thank Editage (www.editage.com) for English language editing. This work was supported by Grants-in-Aid for Scientific Research (KAKENHI) (Grant No. JP18K13498, JP19H01818, JP19H00651) from the Japan Society for the Promotion of Science (JPSJ), by JSPS KAKENHI on Innovative Areas “Quantum Liquid Crystals” (Grant No. JP19H05826), by the Center of Innovation

Program from the Japan Science and Technology Agency, JST, and by MEXT Quantum Leap Flagship Program (MEXT Q-LEAP) (Grant No. JPMXS0118068681), Japan.

Author contributions

M. W., T. Suzuki, T. Someya, Y.O., S.M., and K.O. performed the TARPES measurements. M. W. performed the data analysis. M.F., T.K., and J.I. conducted maintenance of the HHG laser system and improvements of the TARPES apparatus. M. W., T. Suzuki, and K.O. wrote the manuscript. T. Saitoh, S. S. and K.O. designed the project. All the authors discussed the results and contributed to the manuscript.

Data availability

The data supporting the findings of this study are available from the corresponding author upon request.

Competing interests

The authors declare no competing interests.

*Corresponding author.

takeshi.suzuki@issp.u-tokyo.ac.jp

†Corresponding author.

okazaki@issp.u-tokyo.ac.jp

References

1. Zhou, J. S., Goodenough, J. B., Dabrowski, B., Klamut, P. W. & Bukowski, Z. Enhanced susceptibility in LNiO3 perovskites (L = La, Pr, Nd, Nd0.5Sm0.5). *Phys. Rev. Lett.* **84**, 526–529 (2000).
2. Zhou, J. S., Marshall, L. G. & Goodenough, J. B. Mass enhancement versus Stoner enhancement in strongly correlated metallic perovskites: LaNiO3 and LaCuO3. *Phys. Rev. B.* **89**, 245138 (2014).
3. Nahory, R. E., Pollack, M. A., Johnston, W. D. & Barns, R. L. Band gap versus composition and demonstration of Vegard's law for In1 – xGaxAsyP1–y lattice matched to InP. *Appl. Phys. Lett.* **33**, 659–661 (1978).
4. Koshihara, S., Tokura, Y., Takeda, K. & Koda, T. Reversible photoinduced phase transitions in single crystals of polydiacetylenes. *Phys. Rev. Lett.* **68**, 1148–1151 (1992).
5. Miyano, K., Tanaka, T., Tomioka, Y. & Tokura, Y. Photoinduced insulator-to-metal transition in a perovskite manganite. *Phys. Rev. Lett.* **78**, 4257–4260 (1997).
6. Collet, E. *et al.* Laser-induced ferroelectric structural order in an organic charge-transfer crystal. *Science.* **300**, 612–615 (2003).

7. Yoshida, R. *et al.* Ultrafast photoinduced transition of an insulating VO2 thin film into a nonrutile metallic state. *Phys. Rev. B.* **89**, 205114 (2014).
8. Morrison, V. R. *et al.* A photoinduced metal-like phase of monoclinic VO2 revealed by ultrafast electron diffraction. *Science.* **346**, 445–448 (2014).
9. Ichikawa, H. *et al.* Transient photoinduced 'hidden' phase in a manganite. *Nat. Mater.* **10**, 101 (2011).
10. Okazaki, K. *et al.* Photo-induced semimetallic states realised in electron-hole coupled insulators. *Nat. Commun.* **9**, 4322 https://doi.org/10.1038/s41467-018-06801-1 (2018).
11. Wilson, J. A. & Yoffe, A. D. The transition metal dichalcogenides discussion and interpretation of the observed optical, electrical and structural properties. *Adv. Phys.* **8**, 193–335 (1969).
12. Sipos, B. *et al.* From Mott state to superconductivity in 1T-TaS2. *Nat. Mater.* **7**, 960–965 (2008).
13. Kusmartseva, A. F., Sipos, B., Berger, H., Forró, L. & Tutiš, E. Pressure induced superconductivity in pristine 1T-TiSe2. *Phys. Rev. Lett.* **103**, 236401 (2009).
14. Navarro-Moratalla, E. *et al.* Enhanced superconductivity in atomically thin TaS2. *Nat. Commun.* **7**, 11043 https://doi.org/10.1038/ncomms11043 (2016).
15. Chen, P. (ed) e*t al.*, Charge density wave transition in single-layer titanium diselenide, *Nat. Commun.* **6**, 8943; 10.1038/ncomms9943 (2015).
16. Stojchevska, L. *et al.* Ultrafast switching to a stable hidden quantum state in an electronic crystal. *Science.* **344**, 177–180 (2014).
17. Straub, T. *et al.* On the Peierls transition in 2H-NbSe2. *Physica B: Condens. Matter.* **259–261**, 981–982 (1999).
18. Rossnagel, K., Rotenberg, E., Koh, H., Smith, N. V. & Kipp, L. Fermi surface, charge-density-wave gap, and kinks in 2H-TaSe2. *Phys. Rev. B.* **72** (R), 121103 (2005).
19. Yokoya, T. *et al.* Fermi surface sheet-dependent superconductivity in 2H-NbSe2. *Science.* **294**, 2518–2520 (2001).
20. Rahn, D. J. *et al.* Gaps and kinks in the electronic structure of the superconductor 2HNbSe2 from angle-resolved photoemission at 1 K. *Phys. Rev. B.* **85**, 224532 (2012).
21. Kiss, T. *et al.* Charge-order-maximized momentum-dependent superconductivity. *Nat. Phys.* **3**, 720–725 (2007).
22. Torchinsky, D. H., Chen, G. F., Luo, J. L., Wang, N. L. & Gedik, N. Band-dependent Quasiparticle Dynamics in Single Crystals of the Ba0.6K0.4Fe2As2 Superconductor Revealed by Pump-Probe Spectroscopy. *Phys. Rev. Lett.* **105**, 027005 (2010).
23. Mansart, B. *et al.* Coupling of a high-energy excitation to superconducting quasiparticles in a cuprate from coherent charge fluctuation spectroscopy, Proc. Natl. Acad. Sci. USA 110, 4539(2013).
24. Okazaki, K. *et al.* Antiphase Fermi-surface modulations accompanying displacement excitation in a parent compound of iron-based superconductors, Phys. Rev. B 97, 121107(R)(2018).
25. Suzuki, T. *et al.* Photoinduced possible superconducting state with long-lived disproportionate band filling in FeSe. *Commun. Phys.* **2**, 115 https://doi.org/10.1038/s42005-019-0219-4 (2019).

26. Rohwer, T. *et al.* Collapse of long-range charge order tracked by time-resolved photoemission at high momenta. *Nature.* **471**, 490 (2011).
27. Hellmann, S. *et al.* Time-domain classification of charge-density-wave insulators. *Nat. Commun.* **3**, 1069 https://doi.org/10.1038/ncomms2078 (2012).
28. Zeiger, H. J. *et al.* Theory for displacive excitation of coherent phonons. *Phys. Rev. B.* **45**, 768 (1992).
29. Blaha, P., Schwarz, K., Madsen, G. K. H., Kvasnicka, D. & Luitz, J. *WIEN2K, An Augmented Plane Wave + Local Orbitals Program for Calculating Crystal Properties* (Karlheinz Schwarz, Techn. Universität Wien, Austria, 2001).
30. Perfetti, L. *et al.* Ultrafast Electron Relaxation in Superconducting Bi2Sr2CaCu2O8 + d by Time-Resolved Photoelectron Spectroscopy. *Phys. Rev. Lett.* **99**, 197001 (2007).
31. See Supplementary Material
32. Tsang, J. C., Smith, J. E. & Shafer, M. W. Raman spectroscopy of soft modes at the charge-density-wave phase transition in 2H-NbSe2. *Phys. Rev. Lett.* **37**, 1407 (1976).
33. Sooryakumar, R., Klein, M. V. & Frindt, R. F. Effect of nonmagnetic impurities on the Raman spectra of the superconductor niobium diselenide. *Phys. Rev. B.* **23**, 3222 (1981).

Figures

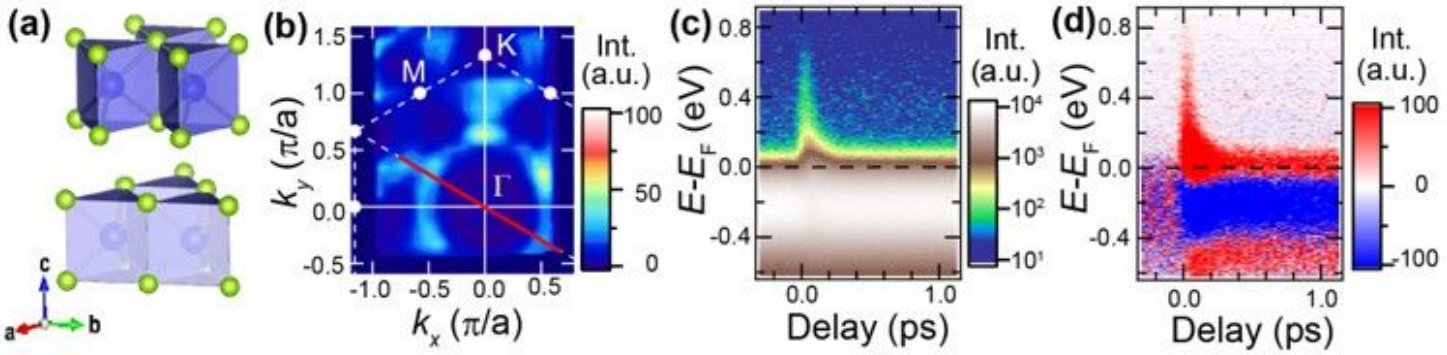

Figure 1

(a) Crystal structure of 2H-NbSe2. (b) ARPES intensity map measured from a He discharge lamp (hv = 21 eV). The intensity is integrated within ±10 meV from EF. (c) Row and (d) differential spectra of the TARPES intensity map with respect to energy and pump-probe delay. They are integrated along the red line in Fig. 1 (b).

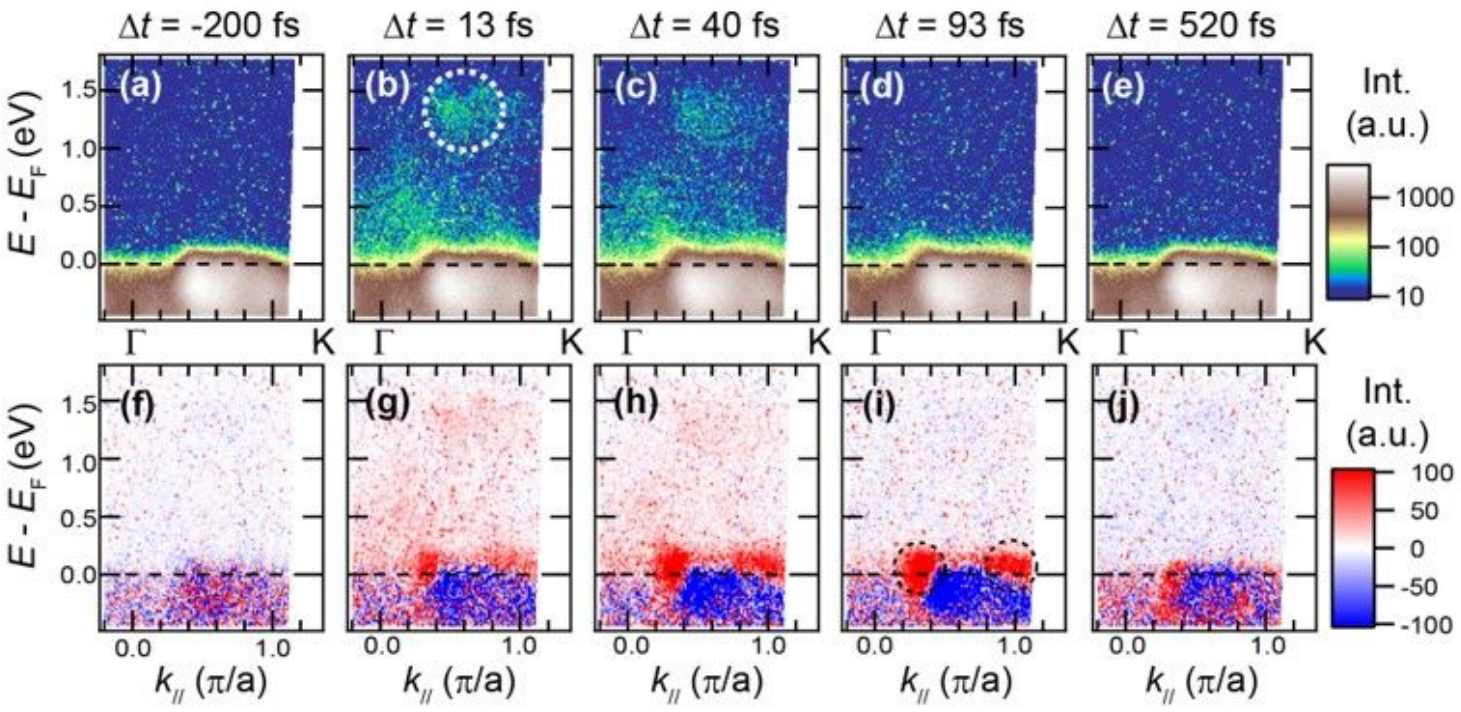

Figure 2

(a)–(e) Row and (f) –(j) difference ARPES snapshots at the delay times indicated above. The time delays at which (f)–(j) were measured correspond to those in (a)–(e) respectively. All data were measured along the ΓK direction.

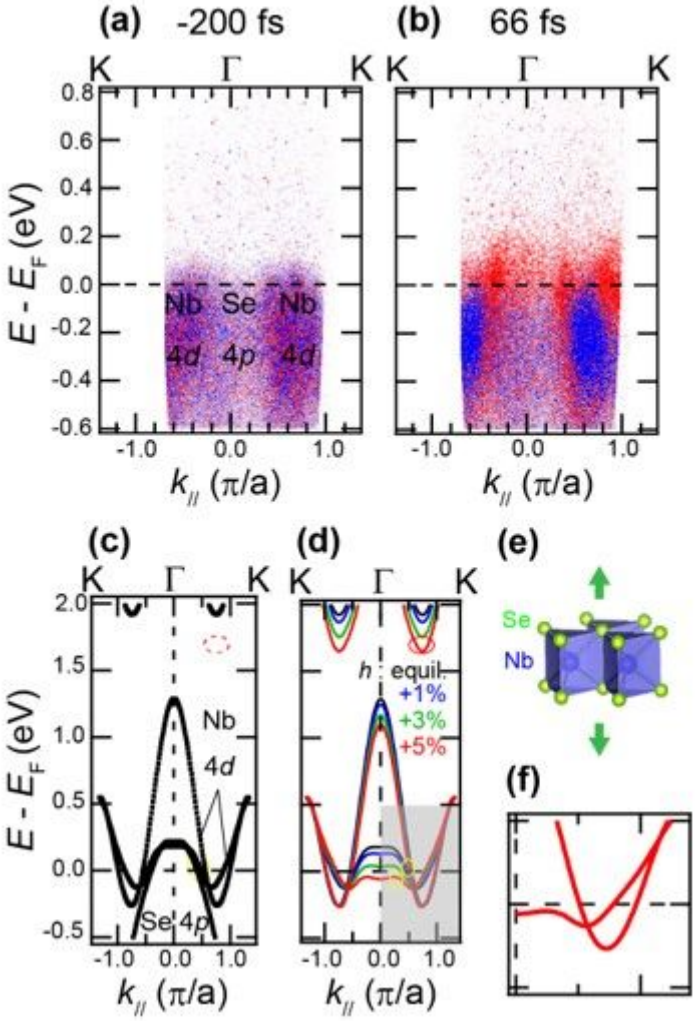

Figure 3

ARPES spectra (a) before optical pumping and (b) at 66 fs. (c) Equilibrium band structure via DFT-GGA calculations. (d) Variation of band structure due to lattice modulation shown in (e). (f) Magnified band structure corresponding to the area indicated by the gray hatch in (d).

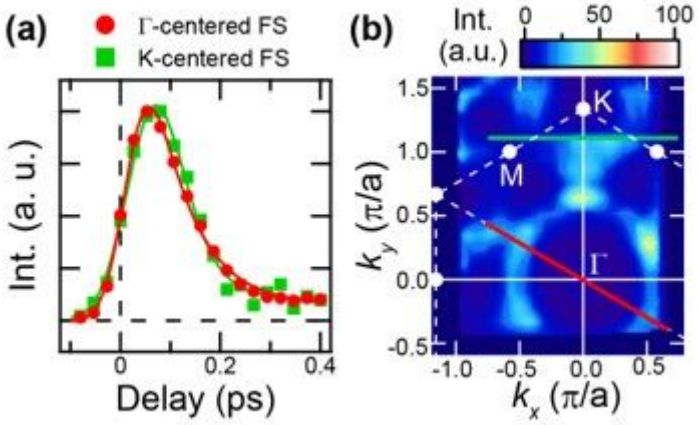

Figure 4

(a) Time dependence of the momentum-integrated intensity of FSs around the Γ and K points. The markers are the experimental data while the lines are fits. The energy window is set to be from EF to + 0.8 eV. (b) Fermi surface map. The red and green lines correspond to the momentum regions integrated for Γ- and K-centered FSs in (a).

Supplementary Files

This is a list of supplementary files associated with this preprint. Click to download.

- NbSe2SMfin.pdf